Influence of present day and glacial surface conditions on the Antarctic Oscillation/Southern Annular Mode

Flávio Justino[1,2] and W. Richard Peltier[1]

[1] Based upon coupled climate simulations driven by present day and glacial boundary conditions, we demonstrate that the internal variability associated with the pronounced south polar climate anomalies that characterized the glacial climate regime was largely confined to the winter season. In particular, the intensity and spatial structure of the Antarctic Oscillation/Southern Annular Mode is found to display a strong seasonal cycle. In the summer season, we demonstrate that this mode of internal climate variability is extremely robust in response to a change from modern to glacial conditions in that it seems not to depend upon the latitudinal position of the baroclinic zone nor on the strength of the mean atmospheric zonal circulation. In winter, however, and under glacial conditions, this mode is characterized by a significantly modified atmospheric circulation that differs dramatically in terms of its internal variability from that characteristic of modern conditions. **Citation:** Justino, F., and W. R. Peltier (2006), Influence of present day and glacial surface conditions on the Antarctic Oscillation/Southern Annular Mode, *Geophys. Res. Lett.*, *33*, L22702, doi:10.1029/2006GL027001.

1. Introduction

[2] Earth's climate system exhibits several internal modes of variability that are characterized by distinct temporal and spatial patterns. In the tropical region and at interannual time scales, climate conditions are strongly modulated by ENSO (El Niño Southern Oscillation) phases [e.g., *Feldstein*, 2000]. Over midlatitudes and the northern hemisphere (NH) polar region, however, the climate regime is mainly dictated by vacillation in the phase of the NAM/AO (Northern Annular Mode/Arctic Oscillation) [e.g., *Rogers*, 1990; *Wallace and Gutzler*, 1981]. The Southern Hemisphere (SH) dominant pattern of climate variability is the SAM/AAO (Southern Annular Mode/Antarctic Oscillation) which appears to be linked to latitudinal migration of the subtropical upper-level jet and variations in the intensity of the polar jet [*Carvalho et al.*, 2005; *Gong and Wang*, 1999]. This, in turn, affects SH surface conditions via associated changes in the momentum and heat budgets. Although modeling efforts and observation based analyses have shed some light on the SAM on interannual to decadal time scales, several issues remain unclear. For instance, there is widespread disagreement [e.g., *Visbeck and Hall*, 2004;

White, 2004], concerning the influence of surface conditions in generating transitional phases and in determining the temporal robustness of the SAM. Moreover, there is evidence that the SAM is tightly linked to the ENSO process [e.g., *L'Heureux and Thompson*, 2006; *Fogt and Bromwich*, 2006] as well as to the Antarctic circumpolar wave [*White*, 2004].

[3] The impact of changes in surface climate conditions (e.g., land ice, sea ice and surface temperature distributions) on the SAM may be usefully investigated on the basis of climate experiments designed to inter-compare the nature of this mode of variability under Last Glacial Maximum (LGM) and modern conditions. Since LGM climate was characterized by very significant changes of SH sea ice extent and extremely cold conditions around the Antarctic Peninsula [e.g., *Peltier and Solheim*, 2004], it might be expected that significantly different SAM variability would be characteristic of these two epochs. Furthermore, the results of some previous modeling studies have strongly suggested an amplification of ENSO variance during the LGM [*Peltier and Solheim*, 2004; *An et al.*, 2004]. This raises the possibility of the existence of distinct teleconnection regimes between ENSO and the SAM depending upon the epoch of interest. The existence of these changes of tropical and polar oceanic surface conditions therefore provides an unique opportunity to study the importance of climate feedbacks on SH polar climate variability.

2. Coupled Climate Simulations

[4] In order to investigate the relationship between the SAM and south polar surface conditions (e.g., sea ice, land surface topography and surface temperature), two model simulations have been performed with the low resolution version of the NCAR-CSM 1.4 model. A modern simulation driven by present day boundary conditions (MOD) and a second experiment for the LGM. Since these experiments have been described in detail elsewhere [*Peltier and Solheim*, 2004] no purpose will be served by providing further description herein. These simulations were run to equilibrium for 2000 (2500) years and the analyses discussed herein are based upon the last 500 years of each simulation.

[5] It is important to note that the inclusion of the LGM ice sheet topography of the ICE-4G model [*Peltier*, 1994] leads to highly significant changes in the height of the West Antarctica ice sheet. In the LGM simulation West Antarctica is approximately 1000 m higher as compared to the MOD simulation. The reduction of atmospheric CO_2 concentration to 200 ppm characteristic of the LGM state and the change of the orbital configuration, moreover, lead to a

---

[1]Department of Physics, University of Toronto, Toronto, Ontario, Canada.

[2]Now at Departamento de Engenharia Agrícola, Universidade Federal de Viçosa, Viçosa, Brasil.
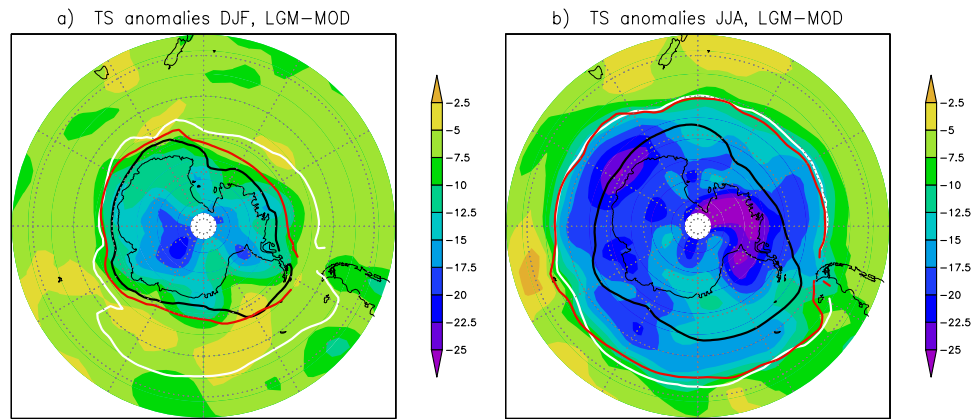
Figure 1. Surface temperature anomalies between MOD and LGM simulations: (a) DJF and (b) JJA [K]. The white (black) line shows the sea ice margin for LGM (MOD) conditions. The red line pertains to GLAMAP reconstruction.

marked expansion of SH sea ice extent, as also discussed by *Shin et al.* [2003].

[6] We will focus herein upon the winter (June, July and August, JJA) and summer (December, January and February - DJF) seasons of the SH. In DJF, surface temperature anomalies over Antarctica between the MOD and LGM simulations approach a magnitude of $-20°C$ (Figure 1a). One should keep in mind that despite this substantial cooling the SH climate symmetry is not affected. The glacial cooling is due primarily to the combined direct and indirect influences of lapse-rate in the low atmospheric CO_2 concentration environment. These anomalies in general follow the changes in glacial topography, in particular the enhanced topographic height over West Antarctica. In addition, the radiative cooling associated with a dryer atmosphere further enhances polar cooling. According to *Weatherly et al.* [1998] the CSM 1.4 predicted air temperatures over sea ice in the SH exhibit cold biases of $2-4$ K.

[7] Turning to changes in the austral winter (Figure 1b), it is evident that an intense cooling has occurred under glacial conditions as compared with modern. Furthermore, SH cooling also extends significantly northward over mid-latitudes. Although the lapse rate effect still plays a crucial role in generating the JJA cooling, we argue that these strong negative anomalies in the LGM simulation are more likely a result of: 1. the substantial increase of sea ice area which inhibits the transfer of heat from the ocean to the overlying atmosphere; 2. the advection of cold air from the elevated ice sheet that leads to additional cooling over the Antarctic Peninsula. By investigating modern polar climate, *Weatherly et al.* [1998] have shown that the predicted ice-covered area and ice thickness in the CSM model are close to observations in the SH. They emphasize, furthermore, that the interannual variability of the ice area is similar to that revealed by satellite measurements. The sea ice margin positions in the LGM and MOD simulations (Figures 1a and 1b) reveal the substantial increase of sea ice extent in both seasons under LGM conditions. It is also clear that compared with the GLAMAP data set (red line in Figures 1a and 1b) our LGM simulation overestimates the sea ice extent in DJF. In JJA, however, our results are in close accord with this recent sea ice reconstruction for LGM conditions [*Pflaumann et al.*, 2003]. Moreover, there is an increase of sea ice thickness in the Weddell and Ross Seas

under LGM conditions (not shown). In contrast with DJF conditions, in JJA it is evident that changes of the symmetry of the SH surface temperature field occurs with extremely cold conditions in West Antarctica and milder conditions in East Antarctica. As will be discussed in what follows this leads to substantial changes of the glacial winter SAM.

[8] In addition to changes of sea ice and surface temperature, the incorporation of the LGM boundary conditions changes the geopotential height distribution at 500 hPa (Z500) as compared to the modern simulation (Figure 2). The main observed features of the present day stationary waves in the SH polar region are reasonably reproduced in our MOD simulation. Clearly evident is the trough (ridge) over the eastern (western) part of the hemisphere (Figures 2a and 2c). It should be noted that the simulated trough in MOD is more meridionally confined as compared to the NCEP dataset [*Kalnay et al.*, 1996]; and that the main center of action of Z500 over the Pacific Ocean in JJA is overestimated in its intensity. Seasonal changes of Z500 (Figure 2) over the mainland of Antarctica are primarily due to a reduction of the thickness of the column due to enhanced lower tropospheric cooling in JJA (Figure 1). Given these changes of atmospheric and oceanic conditions and according to the thermal wind relation, an intensification of the westerly flow is to be expected in the LGM simulation. This has been found to be the case; calculation of the total kinetic energy ($E = \frac{1}{2}(v^2 + u^2)$, not shown) reveals a substantial strengthening of surface winds as well as of the sub-tropical and polar jets in both seasons. Based upon comparison of SH climate conditions between present day and LGM, in what follows we investigate the impact of these differences upon the temporal and spatial structure of the SAM.

3. Temporal and Spatial Climate Variability

[9] Based on empirical orthogonal function (EOF) and spectral analysis performed on monthly data and in agreement with previous studies [e.g., *L'Heureux and Thompson*, 2006; *Kushner et al.*, 2001], the SAM is herein first displayed in terms of the spatial pattern of its amplitude (Figure 3), obtained by regressing the hemispheric Z500 anomalies upon the monthly leading principal component (PC) time series from the SH domain between $20°$ and $88°S$
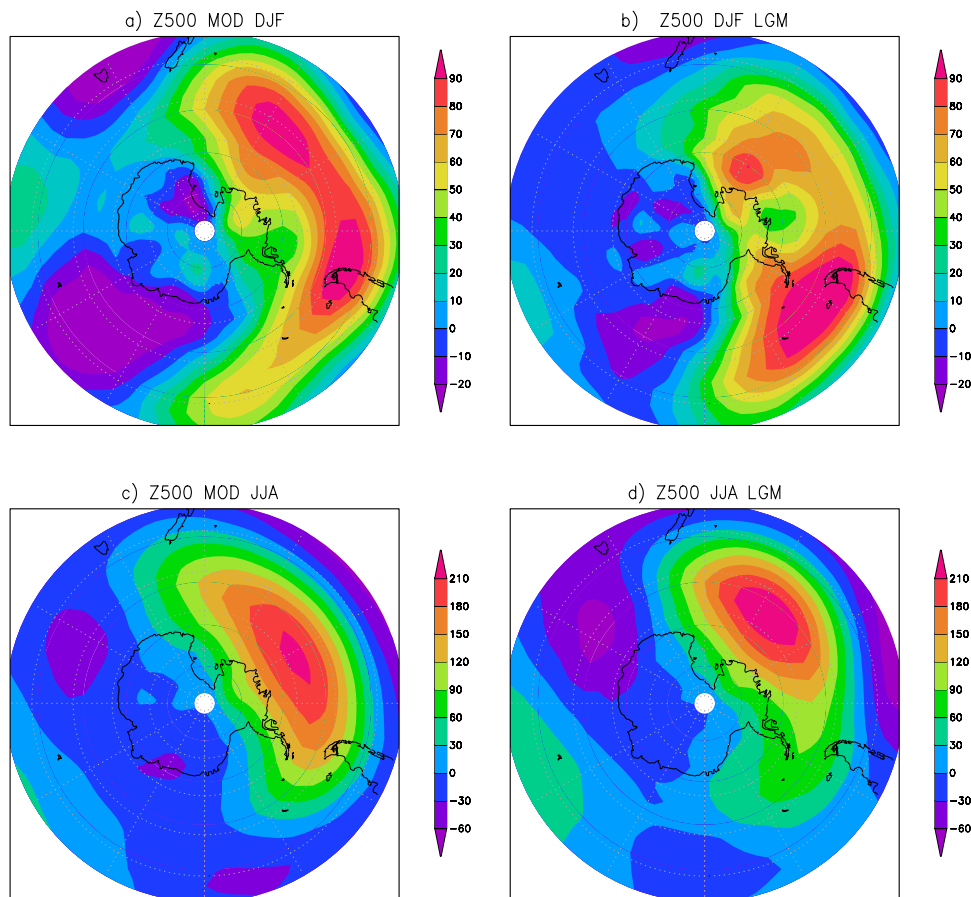
Figure 2. Eddy geopotential height at 500 hPa [meters] (i.e. geopotential height with the zonal mean removed) (a) in DJF and (c) in JJA for MOD simulation. (b and d) Same as in Figures 2a and 2c but for LGM simulations.
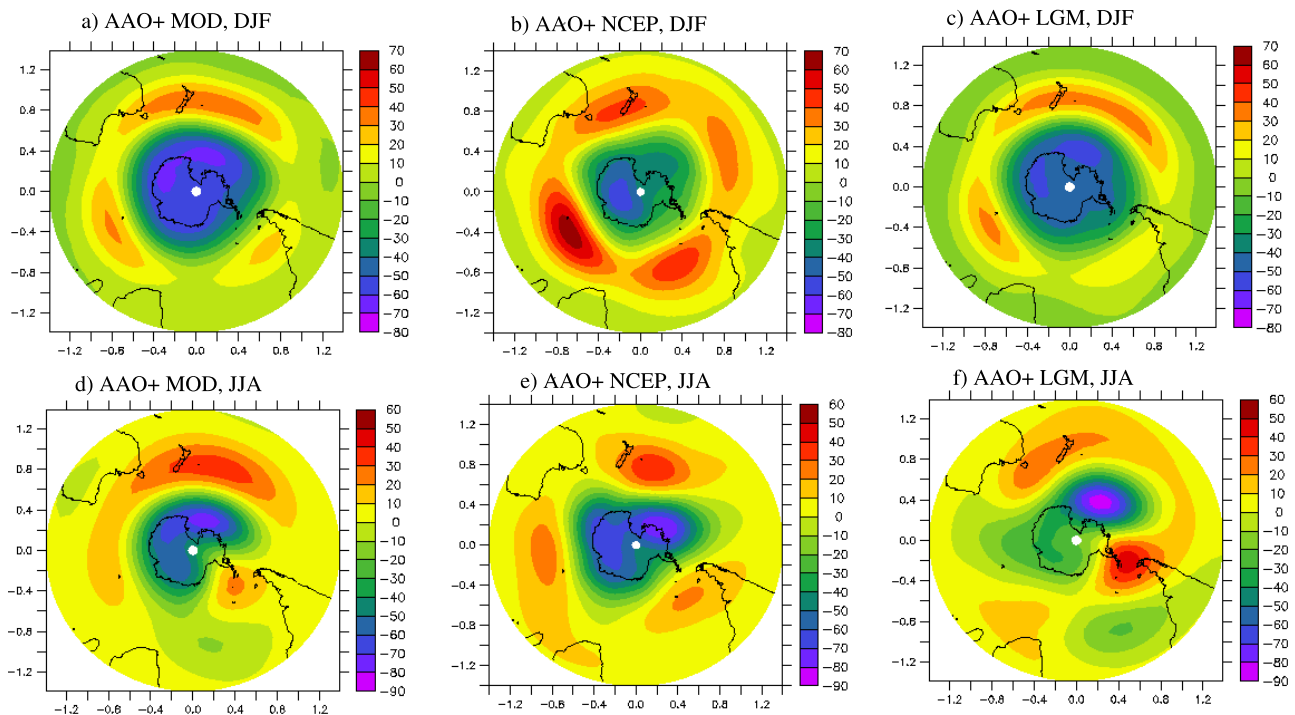
Figure 3. SAM (a) in DJF and (d) in JJA for MOD simulation. (b and e) Same as in Figures 3a and 3d but for NCEP dataset [meters]. (c and f) SAM/GSM for LGM simulation in DJF and JJA.

latitude. The EOF is computed in DJF and JJA for both MOD and LGM runs. The 500 hPa geopotential height level was chosen to avoid intersection with Antarctic topography. The leading pattern of variability in the MOD simulation (Figure 3a) is characterized by the existence of a well known characteristic annular structure over the entire hemisphere, which is dominated by two areas of strongest out-of-phase variability located over mid-latitudes (40°–55°S) and the polar region. For comparison we show in Figure 3b the SAM based on the NCEP dataset. Although differences are clearly identified between the modeled and observed SAM, it is evident that the CSM provides a satisfactory depiction of this atmospheric mode. When all months are used in the EOF calculation the modeled and observed SAM exhibit a characteristic wave number 3 (not shown). The first modeled (NCEP) EOF for DJF (Figure 3) accounts for 39% (36%) of the total variance and is well separated from the second EOF which explains 9% (10%). One should keep in mind that these results are different as compared with analyses performed on seasonal mean anomalies rather than monthly data. Because intra-seasonal variability is not captured if seasonal mean data is employed, seasonal mean SAM representation displays an even more annular structure (not shown). It has been found, moreover, that the spatial pattern of the SAM computed at 500 hpa is similar to the SAM computed at sea level, a fact that usefully serves to highlight its barotropic nature. Figure 3d demonstrates that the modern SAM (first EOF of Z500) in austral winter is no longer characterized by a predominant annular structure and explains less variance (20%) as compared with the result for the summer season. In fact, the wintertime structure of the modern SAM is characterized by centers of action that somewhat resemble the Antarctic Dipole (ADP) as defined by *Yuan and Martinson* [2000], which is characterized by a zonal seesaw in sea ice and SLP -as well as other indices-between the eastern Pacific and Atlantic sectors of the Antarctic continent. Indeed, our simulations display an anomalous sea ice thickness and SST response that are dependent upon the phase of the SAM (not shown). Although there is still much to be learned concerning the cause of the seasonal variability of the AAO, *Bromwich et al.* [1998] argued that any change of meridional circulation induced by variations of tropical SST or/and sea ice may lead to distinct polar climate variability.

[10] In order to study the glacial SAM, identical EOF analyses were performed on the results obtained from the LGM simulation. The first EOF in DJF in the LGM run explains 29% of the total variance. Despite markedly different surface climate conditions in the LGM simulation during the summer season compared to the modern simulation (see Figure 1), the EOF results reveal that there is no substantial change in the form of the glacial SAM (Figure 3c). This was not anticipated since the LGM simulation is characterized by a significant difference in the meridional thermal gradient, a shift in the latitudinal position of the baroclinic zone and intensified wind shear. The EOF analyses for austral winter, however, exhibit a markedly different structure in which the first EOF explains only 19% of the total variance (Figure 3f). Moreover, by comparing Figure 3d with Figure 3f it is clear that in JJA the modified glacial surface conditions do lead to a distinctive leading pattern of variability under LGM conditions. In

particular, the annular structure is completely absent and a wave train is predicted to dominate the polar mode of variability. Given this, hereafter this mode will be referred as the Glacial Southern Mode (GSM) rather than the SAM. It should be noted that the GSM strongly resembles the ENSO/Pacific South American mode as identified by *Mo and Higgins* [1998]. The centre of action of Z500 anomalies over the central Pacific that is characteristic of the present day SAM (Figure 3d) is weakened and shifted westward over the Australia/New Zealand region under LGM conditions (Figure 3f). The GSM is dominate by two areas of strongest variability respectively over the Drake passage and around the dateline. It should be noted that *Yuan and Martinson* [2000] have associated the dominant interannual variance structure in the sea ice edge and surface air temperature/atmospheric pressure in the circumpolar Antarctic region to tropical ENSO events. Since some previous modelling studies have suggested, at least in CSM 1.4, that the strength of the ENSO phenomenon was significantly increased under LGM conditions [*Peltier and Solheim*, 2004; *An et al.*, 2004], one may expect that this interaction would be strengthened under LGM conditions. It will be interesting to investigate the robustness of this result using a new simulation of LGM climate using the CCSM 3 version of the NCAR model since in this model the ENSO process seems to be weaker under LGM conditions rather than stronger.

[11] Our final focus in this paper is upon the temporal variability of the SAM/GSM. In order to perform the spectral analysis of the Principal Components (PC) time series by applying the Multi-Taper method (MTM), 3 tapers were employed and spectral fluctuations at frequencies greater than the Rayleigh frequency are thereby well resolved (for details see *Thomson* [1982]). Calculation of the power spectrum of the first PC time series of Z500 in DJF and JJA, does not reveal any dominant temporal variability, as the SAM/GSM at 500 hPa shows a power spectrum essentially dominated by white noise (not shown). Therefore, Figure 4 shows the power spectrum of the SAM/GSM calculated at sea level. These results will prove useful for analysis of the ENSO-SAM/GSM interplay. Based upon Figure 4a it is clear that the SAM/GSM exhibits some concentration of power at interannual timescales of 3–5 years period which is dominant (red noise). It should be noted that although the SAM displays a similar spatial pattern at 500 hPa and sea level, the power spectra are different depending on the level chosen. The 3–5 year peak is also evident when the power spectrum is computed for half the full length of the record, thus demonstrating the robustness of the inter-annual signal. This result agrees with previous analyses based upon tree-ring derived proxy climate time series and the longest surface pressure time series available in the South American-Antarctic Peninsula sector [*Villalba et al.*, 2001], insofar as the existence of the interannual signal is concerned. Supporting evidence for the existence of variability in the 2–5 year period range was obtained by *Visbeck and Hall* [2004] and *White* [2004]. Based on our modeling results, one may conclude that the signal with ENSO periodicity is not propagated into the middle troposphere. It may be important to note that *Kushner et al.* [2001] have pointed out the possible involvement of the upper troposphere/lower stratosphere in the
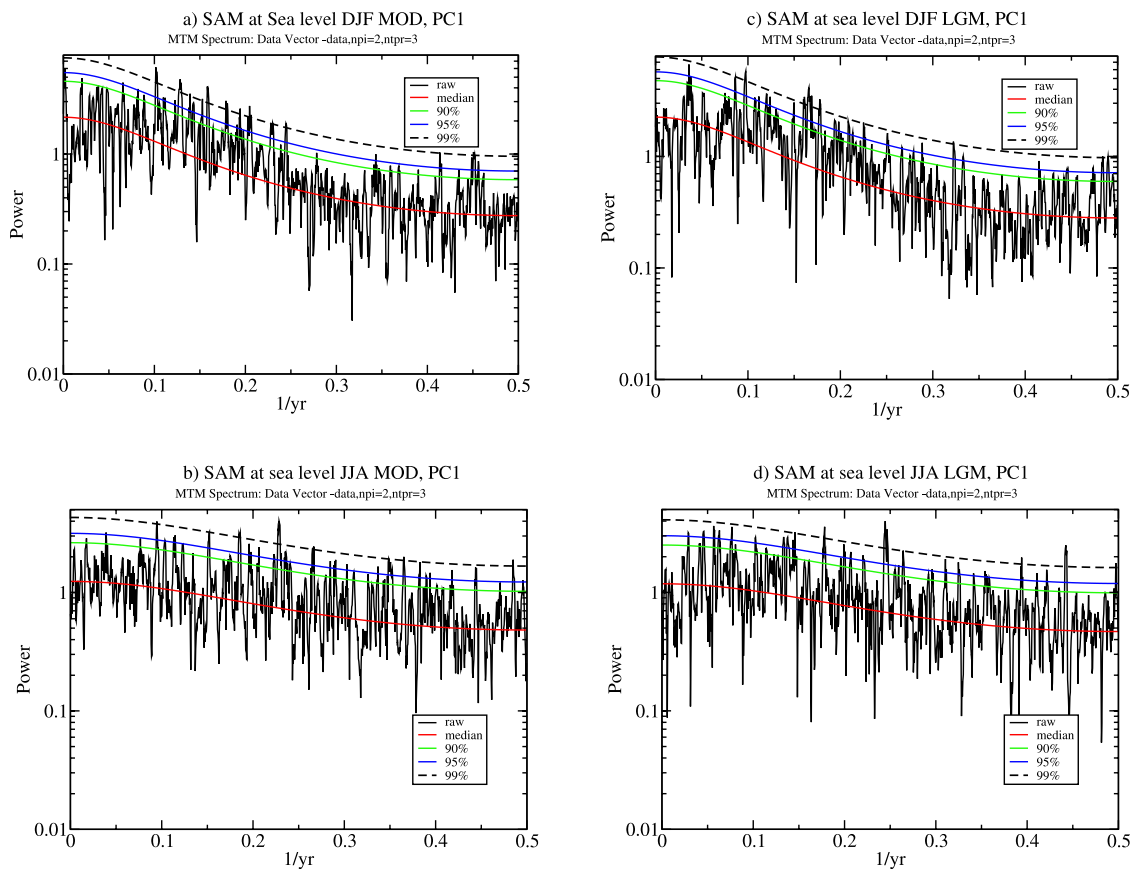
Figure 4. MTM power spectrum for the first PC of SLP in the MOD and LGM simulations (a) in DJF and (b) in JJA for the MOD simulation. (c and d) Same as in Figures 4a and 4b but calculated for the LGM run. Also shown is the corresponding confidence levels (smooth lines), 90%, 95% and 99% for significance relative to the null hypothesis (red noise).

control of SAM variability. This could conceivably contribute to the damping of ENSO influence at 500 hPa.

[12] The incorporation of LGM boundary conditions does not lead to a distinct form of temporal variability of the glacial SAM/GSM as compared to the MOD simulation (Figures 4c and 4d). It has been previously recognized that under modern conditions intraseasonal and interannual variability in the tropics occurs in phase with distinct polarities of the SAM [e.g., *L'Heureux and Thompson*, 2006; *Carvalho et al.*, 2005; *Bromwich et al.*, 1998]. At the heart of this teleconnection is the ENSO phenomenon. To provide an initial investigation of the interplay between the present day SH extratropical atmosphere and ENSO, which in our model supports a $2-4$ year quasi-periodic signal, we have computed the lag correlation between the first principal component (PC1) of the SAM/GSM index and the PC1 of SST computed in the tropical Pacific ($20°S-20°N$) for modern and LGM conditions (not shown). This analysis demonstrates that in DJF, at lag 0, accompanying the positive amplitude phase of the SAM, the equatorial Pacific cools. Nevertheless, our analyses reveal that there is no substantial correlation between those indexes under present day conditions. In the same way, during JJA the PC1 of SST and the SAM index are barely correlated because ENSO power in the MOD simulation, as well as its climate teleconnection, is much weaker during JJA. Turning to analyses of the LGM conditions, it is interesting

to note the significantly higher correlation (a maximum value of 0.4) between the leading PC of SST in the tropical Pacific and the GSM. Given this, one may argue that the tropical-extratropical teleconnection was enhanced during the LGM period. Clearly, additional studies will be required to investigate the climate mechanisms associated with the interaction between ENSO and the SAM/GSM. Moreover, it will prove interesting to investigate the cause of changes in the power spectrum from red noise to white noise according to the atmospheric level.

4. Summary and Concluding Remarks

[13] Through a series of coupled climate simulations performed subject to present day and glacial boundary conditions, our analyses provide evidence that despite substantial changes of sea ice area and surface temperature in the summer season there is no prominent change in the spatial structure of the glacial SAM as compared to the modern SAM. We suggest, therefore, that in general the SAM in DJF is a very robust pattern that does not depend strongly upon the nature of the surface boundary conditions, nor on the position of the baroclinic zone and the mean atmospheric westerly flow. This contrasts with the results of analysis of this mode in JJA which demonstrate that the mode is expected to have been drastically modified during the glacial period. The reason for the significant modifica-

tion to the polar mode in winter is perhaps a consequence of the fact that the symmetry of the surface boundary conditions in the south polar region is changed as a consequence of strongly enhanced cooling over the Antarctic peninsula and adjacent ocean (Figure 1b). Similar results have been reported for the glacial North Atlantic Oscillation as discussed recently by *Justino and Peltier* [2005], in which it was found that the polar climate variability during the LGM is strongly modulated by the direct mechanical effect of ice sheet paleo-topography (lapse rate) and by the effect of diabatic heating due to the marked change in the spatial variation of surface albedo.

References

An, S.-I., A. Timmermann, L. Bejarano, F.-F. Jin, F. Justino, Z. Liu, and A. W. Tudhope (2004), Modeling evidence for enhanced El Niño–Southern Oscillation amplitude during the Last Glacial Maximum, *Paleoceanography*, *19*, PA4009, doi:10.1029/2004PA001020.

Bromwich, D., B. Chen, K. M. Hines, and R. I. Cullather (1998), Global atmospheric responses to Antarctic forcing, *Ann. Glaciol.*, *27*, 521–527.

Carvalho, L. M. V., C. Jones, and T. Ambrizzi (2005), Opposite phases of the Antarctic Oscillation and relationships with intraseasonal to interannual activity in the tropics during the austral summer, *J. Clim.*, *18*, 702–718.

Feldstein, S. B. (2000), Teleconnections and ENSO: The timescale, power spectra, and climate noise properties, *J. Clim.*, *13*, 4430–4440.

Fogt, R., and D. H. Bromwich (2006), Decadal variability of the ENSO teleconnection to the high latitude South Pacific governed by coupling with the Southern Annular Mode, *J. Clim.*, *19*, 979–999.

Gong, D., and S. Wang (1999), Definition of Antarctic oscillation index, *Geophys. Res. Lett.*, *26*, 459–462.

Justino, F., and W. R. Peltier (2005), The glacial North Atlantic Oscillation, *Geophys. Res. Lett.*, *32*, L21803, doi:10.1029/2005GL023822.

Kalnay, E., et al. (1996), The NCEP-NCAR 40 year reanalysis project, *Bull. Am. Meteorol. Soc.*, *77*, 437–471.

Kushner, P. J., I. M. Held, and T. L. Delworth (2001), Atmospheric circulation response to global warming, *J. Clim.*, *14*, 2238–2249.

L'Heureux, M. L., and D. W. J. Thompson (2006), Observed relationships between the El Niño Southern Oscillation and the Extratropical Zonal–Mean Circulation, *J. Clim.*, *19*, 276–287.

Mo, K. C., and W. Higgins (1998), The Pacific–South American modes and tropical convection during the Southern Hemisphere winter, *Mon. Weather Rev.*, *126*, 1581–1596.

Peltier, W. (1994), Ice age paleotopography, *Science*, *265*, 195–201.

Peltier, W., and L. Solheim (2004), The climate of the Earth at Last Glacial Maximum: Statistical equilibrium state and a mode of internal variability, *Quat. Sci. Rev.*, *23*, 335–357.

Pflaumann, U., et al. (2003), Glacial North Atlantic: Sea-surface conditions reconstructed by GLAMAP 2000, *Paleoceanography*, *18*(3), 1065, doi:10.1029/2002PA000774.

Rogers, J. C. (1990), Patterns of low-frequency monthly sea-level pressure variability (1899–1986) and associated wave cyclone frequencies, *J. Clim.*, *3*, 1364–1379.

Shin, S. I., Z. Liu, B. L. O. Bliesner, E. C. Brady, J. E. Kutzbach, and S. P. Harrison (2003), A simulation of the Last Glacial Maximum Climate using the NCAR CSM, *Clim. Dyn*, *20*, 127–151.

Thomson, D. J. (1982), Spectrum estimation and harmonic analysis, *Proc. IEEE*, *70*(9), 1055–1094.

Villalba, R., J. A. Boninsegna, A. Lara, and S. Delgado (2001), Decadal-scale climatic variability in the South American sector of the Southern Ocean: Evidence from tree-ring records during the past four centuries, paper presented at Tree Rings and People: An International Conference on the Future of Dendrochronology, Swiss Fed. Res. Inst., Davos, Switzerland, 22–26 Sept.

Visbeck, M., and A. Hall (2004), Comments on "Synchronous variability in the southern hemisphere atmosphere, sea ice, and ocean resulting from the annual mode"—Reply, *J. Clim.*, *17*, 2255–2258.

Wallace, J. M., and D. Gutzler (1981), Teleconnections in the geopotential height field during the Northern Hemisphere winter, *Mon. Weather Rev.*, *109*, 784–812.

Weatherly, J. W., B. P. Briegleb, and W. G. Large (1998), Sea ice and polar climate in the NCAR CSM, *J. Clim.*, *11*, 1472–1486.

White, W. B. (2004), Comments on "Synchronous variability in the Southern Hemisphere atmosphere, sea ice, and ocean resulting from the annular mode", *J. Clim.*, *17*, 2249–2254.

Yuan, X. J., and D. G. Martinson (2000), Antarctic sea ice extent variability and its global connectivity, *J. Clim.*, *13*, 1697–1717.

————————————

F. Justino, Departamento de Engenharia Agricola, Universidade Federal de Viçosa, Viçosa, P.H. Rolfs 36570 000, Brasil. (fjustino@atmosp.physics.utoronto.ca)

W. R. Peltier, Department of Physics, University of Toronto, 60 St. George Street, Toronto, Ont, Canada M5S 1A7.